Supporting Information

for

Three-Dimensional Orientation Determination of Stationary Anisotropic Nanoparticles with Sub-Degree Precision under Total Internal Reflection Scattering Microscopy

*Kyle Marchuk and Ning Fang**

Ames Laboratory-USDOE and Department of Chemistry, Iowa State University,

Ames, Iowa, 50011

*To whom correspondence should be addressed. Email: nfang@iastate.edu.

Methods

TIRS/TIRF Microscope

The instrument is a home built variable-angle total internal reflection scattering microscope that was modified from previous TIRS and TIRF microscopy applications.[1-4]

The prism-based TIRS instrument was built around a Nikon Optihot-2 microscope, of which the original stage was removed and replaced with a Sutter MP-285 motorized 3D translational stage (Novato, CA). The Sutter stage supported a homemade prism holder that held an equilateral Bk7 prism (Melles Griot, Albuquerque, NM). A 660-nm continuous wave (CW) laser (Ignis, LaserQuantum, San Jose, CA) with an adjustable power output (max 200 mW) was used as the excitation source. The beam was directed through a periscope set of optics, a Uniblitz mechanical shutter (model LS2Z2, Vincent Associates, Rochester, NY), and a focusing lens (15-cm focal length) before being directed to the mirror on a galvanometer optical scanner (model 6220H, Cambridge Technology, Cambridge, MA). The focusing lens was used to control the laser illumination size under the objective, while the mirror galvanometer was used in conjunction with a motorized linear stage (model MAA-PP, Newport, Irvine, CA) to direct the laser beam through the equilateral prism to the solid-liquid interface. The scattered light was collected by an objective (Zeiss, 100x, Adjustable NA 0.7-1.3, oil immersion) before being recorded by an Andor iXon^{EM} + 897 EMCCD (Belfast, Northern Ireland; 512x512 imaging array, 16 μm x 16 μm pixel size). To control the incoming laser polarization a half-wave Fresnel rhomb (FR600HM, Thorlabs, Newton, NJ) was placed into the laser path after the shutter. The Fresnel rhomb was connected to a computer-controlled rotating stage (8MRU-1, Altos Photonics, Bozeman, MT).

The Use of a Double Fresnel Rhomb for Polarization Control

A double Fresnel rhomb rotates the polarization direction by 90° through the use of multiple total internal reflections. Unlike a HWP that uses birefringence to control polarization direction, a double Frensel rhomb will produce elliptically polarized light when it is rotated to angles between 0° and 45° (for each degree rotated the polarization direction rotates by 2°).

Since the light undergoes TIR at the sample, regardless of the polarization circularity, the polarization is broken into s-pol and p-pol components. When the double Fresnel rhomb is

rotated 22.5°, it is producing circularly polarized light, which is translated into half s-pol and half p-pol components at the surface of TIR. The same would be true of the incoming illumination was polarized linearly at ζ=45°. Therefore, while a double Fresnel rhomb cannot be used in many other microscopy techniques to control polarization direction, a TIR illumination scheme is compatible with either a birefringent HWP or a double Fresnel rhomb.

AuNR Orientation Determination

Polarization Rotation. AuNRs (25 nm × 60 nm, aspect ratio 2.4) were purchased from Nanopartz (Salt Lake City, UT). The particles were diluted in a solution of 0.5 (w/v) agarose (Promega, Madison, WI) solution to an appropriate concentration. Hot solution was place on a 2" x 1" quartz microscope slide (SPI Supplies, West Chester, PA) and quickly covered by a 18 mm^2 Corning coverslip. The sample was sealed with enamel and allowed to gel for 30 min at room temperature.

The slide was then placed on the prism and focused under TIRS before being allowed to settle for an additional 30 minutes to reduce sample drift. The double Fresnel rhomb (Thorlabs) HWP was installed onto the rotation stage by the threaded mount taking care to center the laser beam through the HWP. The orientation of the HWP was carefully determined by first placing a polarizer perpendicular to the beam path. The HWP was rotated until maximum extinction occurred determining the horizontal polarization (s-pol).

Data was collected while rotating the polarization direction at 30°/s with a 30 ms camera exposure in frame transfer mode leading to a polarization rotation of 0.9°/frame. Since the control of the rotating stage and our EMCCD is done with separate software, there is a lag of ~30 frames before the rotation was started. Therefore, it is necessary to determine the frame in the movie in which the polarization rotation begins. A AuNR with an approximate polar angle of 45° was chosen to ensure signal change, and a MATLAB program was used to plot the sum of the 10 brightest pixels in a user defined region of interest (ROI) against frame number. The average and standard deviation (σ) intensity of the AuNR was calculated from the first 20 points. When the signal intensity of the AuNR exceeded the average ± 3σ, it indicated that the signal was increasing due to the change in the incoming polarization direction. The first point above this threshold corresponds to the angle ζ = 0.9° and the previous point to ζ = 0.0°.

The first 180° of the polarization rotation is then plot in MATLAB and fit with a multi-order polynomial. The polynomial curve is then used in the fitting with simulations to produce the polar angle of the particle.

Azimuthal Angle Determination. To correctly determine the polar angle, the azimuthal angle (φ) must first be determined. While we mentioned that defocused imaging is unreliable for polar angle determination, a highly accurate azimuthal angle can be obtained from the image. The in-plane angle of the AuNR can be determined from a defocused image by determining the symmetry of the image. The resulting plane of symmetry is then used as the direction of the long-axis of the particle. The simplest way of determining symmetry is to cut the image into two equal area regions around the central point of the image at a variety of angles and determine the intensity in each region. When the intensity difference between the two regions is minimal, the angle will correspond to the angle of symmetry.

As mentioned in the main text, after rotation data are collected for the in-focus AuNR, the procedure is repeated with the sample plane defocused by ~1 μm. The frame in which the intensity for the AuNR is at its maximum is then selected from the stack. A region of interest is drawn around the AuNR and cropped. This image is then loaded into a home written MATLAB code which calculates the symmetry. It should be noted that the line used to cut the image in half is considered infinitely thin and the program will actually cut pixels and assign the appropriate count of intensity to the fractions of the original pixel. Using this technique, no error is generated in integrating the intensity from program.

For each AuNR, an initial image center is chosen manually by visual inspection of the recorded image pattern. The image is divided down the *x* axis through the image center creating two regions (top and bottom), the total intensity of the regions is then summed and the difference is taken. The image is rotated by increments of 0.1° and the process is repeated. The angle that produces the smallest difference between the two regions has the most symmetry and corresponds to the azimuthal angle. Following the symmetry calculations based on the manually assigned image center, similar calculations are carried out for its neighboring pixels. The pixel, at which the integrated intensity difference is the smallest compared to the neighboring pixels, is assigned as the final center point and the corresponding symmetry calculations are used for the final angle of symmetry.

The accuracy of the azimuthal angle determination ultimately depends on the signal of the AuNR and the noise of the image. When the overall signal of the particle is low such as when the AuNR is at the outer edge of the evanescent field or the incoming polarization is not optimized, the background noise will make up a larger fraction of the symmetry regions leading to false orientation assignments. Other false assignments may occur when a AuNR is approaches a near 0° or near 90° polar angle. If the noise component is greater than the subtle differences associated with the particle tilt, actual symmetry may not be determined. Thus, azimuthal angle uncertainty increases the farther the particle is from the surface of TIR, and when the particle reaches nears either extreme in polar angle.

The uncertainty of the angle determination is found by first finding the standard deviation of the background. This is considered the noise of the system. The noise is then multiplied by the area of the image and added to the integrated intensity difference produced at the angle of symmetry. The angles that produce intensity difference less than this intensity value are within the range of uncertainty. A representation of the uncertainty as dependent on total image intensity can be found in the main text in Figure 5.

Simulating Intensity Profiles with Respect to ζ. In order to determine the polar angle of the AuNR, measured scattering intensities have to be compared to calculated data from a theoretical model of the AuNR. Within this model we approximate the particle as an anisotropic electromagnetic dipole $\hat{\mu}$ that scatters photons polarized preferentially along its dipole axis. The scattering intensity, I_s, is related to the dipole vector and the electric field polarization ($\hat{\varepsilon}$):

$$I_s(\hat{\mu}_s, \hat{\varepsilon}) \equiv |\hat{\mu}_s \cdot \hat{\varepsilon}|^2 \tag{1}$$

$$\propto \left(\varepsilon_x^2\mu_x^2 + \varepsilon_y^2\mu_y^2 + \varepsilon_z^2\mu_z^2 + 2\varepsilon_x\varepsilon_y\mu_x\mu_y \sin(\delta_s - \delta_p)\right. \tag{2}$$
$$\left. + \; 2\varepsilon_y\varepsilon_z\mu_y\mu_z \sin(\delta_s - \delta_p)\right)$$

These calculations assume the coordinate system described in the main text where *x* and *y* are the image plane and *x* is the propagation direction of the incident light. The *z* direction is into the microscope objective. The orientation of the AuNR is again described through the polar and azimuthal angle (θ,φ), hence the dipole orientation can be described:

$$\hat{\mu} = (\sin\theta\cos\varphi\,, \sin\theta\sin\varphi\,, \cos\theta) \tag{3}$$

The Cartesian coordinates are thus determined by the magnitude of the *s* and *p* polarization components of the evanescent field. Within our system the *s* component of the overall ε is constrained to the *y* direction. The *p* component of ε is predominantly in the *z* direction, though there is also a component that propagates in the *x* direction. The composition of the evanescent field is described in the following equations:

$$\varepsilon_{p,t} = -2\cos(\zeta)\cos(\theta_i)\sin(\delta_p) \tag{4}$$

$$\varepsilon_{p,n} = 2\cos(\zeta)\sin(\theta_i)\cos(\delta_p)/\xi^2 \tag{5}$$

$$\varepsilon_s = 2\sin(\zeta)\cos(\delta_s) \tag{6}$$

where θ_i is the incident angle of the illuminating laser light, ξ is the ratio of the indices of refraction of the AuNRs surrounding to the slide material, and δ_s and δ_p are the phase lags for *s* and *p* polarized light, respectively.

$$\delta_p = \tan^{-1}\left[\frac{(\sin^2\theta_i - \sin^2\theta_c)^{\frac{1}{2}}}{\sin^2\theta_c\cos\theta_i}\right] \tag{7}$$

$$\delta_s = \tan^{-1}\left[\frac{(\sin^2\theta_i - \sin^2\theta_c)^{\frac{1}{2}}}{\cos\theta_i}\right] \tag{8}$$

where θ_c is the critical angle determined by the indices of refraction of the substrate and sample medium.

Gold Nanorod and Microtubule Co-localization

Microtubule Preparation. Microtubules for AuNR studies were prepared in the following way. Taxol, GTP, and all tubulin were purchased from Cytoskeleton (Denver, CO). Tubulin aliquots were prepared with 86% natural bovine tubulin, 7% rhodamine tagged tubulin, and 7% biotinylated tubulin. The following published protocol was followed:[5, 6] 10 µl BRB80 solution containing 4 mM MgCl2, 0.5 mM GTP, 10 µM Taxol, and 9 µM tubulin was incubated

overnight to reduce the number of short microtubules in solution. 100 µl of BRB80 buffer with 10 µM Taxol was added to stop microtubule nucleation. Microtubules were then resuspended in BRB0 solution supplemented with 10 µM Taxol.

Gold Nanorod Surface Modification. Neutravidin modified gold nanorods were prepared by first centrifuging the AuNR solution for 6 min at 5500 rpm and decanting the supernatant. The particles were then resuspended in 18-MΩ Milli-Q water before a NHS-PEG disulfide link in DMSO (2 mg/ml) was added. Solution was placed on a rotation rack for 90 min. Solution was then diluted to an appropriate concentration with Milli-Q water before neutravidin in PBS (2 mg/ml) was added. The solution was placed on a 3D shaker for a minimum of 2 hours before usage.

AuNR Attachment to Microtubules. The particles were attached to the microtubules by the biotin-neutravidin interaction. This was facilitated by simply mixing an aliquot of microtubules suspended in BRB0 solution supplemented with 10 µM Taxol and an appropriate concentration of AuNRs and incubating for 20 min at room temperature. Gentle vortexing with the thumb periodically can help reduce microtubule clumping. The microtubule-AuNR solution was then placed upon a poly-L-modified glass slide and imaged.

Proximate Neighbor Determinations

An additional advantage of this technique is its ability to distinguish single particles from what has been termed proximate neighbors,[7] meaning multiple uncoupled particles within a diffraction limited spot. The distinction can be made using either the defocused (Supplemental Figure 6) or focused (Supplemental Figure 7) polarization rotation data set. It should be noted that this discussion *does not apply* to the case of plasmon coupling between touching or almost touching plasmonic nanoparticles, which will give rise to different image intensities and patterns.

In Supplemental Figure 6 comparisons are made between two single particles with either a large or small polar angle and a proximate neighbor. The comparisons are made at the polarization orientation of 0° and 90° producing predominantly s-pol and p-pol light at the surface of TIR respectively. As can be seen, the single particles produce a high contrast image in one polarization and nearly no image in the opposing polarization. This is due to the defocused image being independent of the polarization of the illumination source. On the other hand, the

proximate neighbor produces a well-defined defocused image at both polarizations suggesting at least two particles are within the diffraction limited spot size.

The focused polarization rotation data can also be applied in separating single particles from proximate neighbors. Supplemental Figure 7 displays the images of two areas as the polarization direction is rotated 180°. The spot in the left column displays the typical periodic bright to dark intensity response, while the spot in the right column seems to transform from a Gaussian shaped intensity profile to a donut shape. Interpretation of the donut shape indicates a AuNR with a small polar angle is near a AuNR with a large polar angle.

Supplemental References

1. Marchuk, K.; Ha, J. W.; Fang, N. *Nano Letters* **2013,** 13, (3), 1245-1250.
2. Ha, J. W.; Marchuk, K.; Fang, N. *Nano Letters* **2012,** 12, (8), 4282-4288.
3. Marchuk, K.; Guo, Y. J.; Sun, W.; Vela, J.; Fang, N. *Journal of the American Chemical Society* **2012,** 134, (14), 6108-6111.
4. Sun, W.; Marchuk, K.; Wang, G. F.; Fang, N. *Analytical Chemistry* **2010,** 82, (6), 2441-2447.
5. Nitzsche, B.; Ruhnow, F.; Diez, S. *Nature Nanotechnology* **2008,** 3, (9), 552-556.
6. Ray, S.; Meyhofer, E.; Milligan, R. A.; Howard, J. *Journal of Cell Biology* **1993,** 121, (5), 1083-1093.
7. Stender, A. S.; Wang, G. F.; Sun, W.; Fang, N. *Acs Nano* **2010,** 4, (12), 7667-7675.

Supplemental Figures

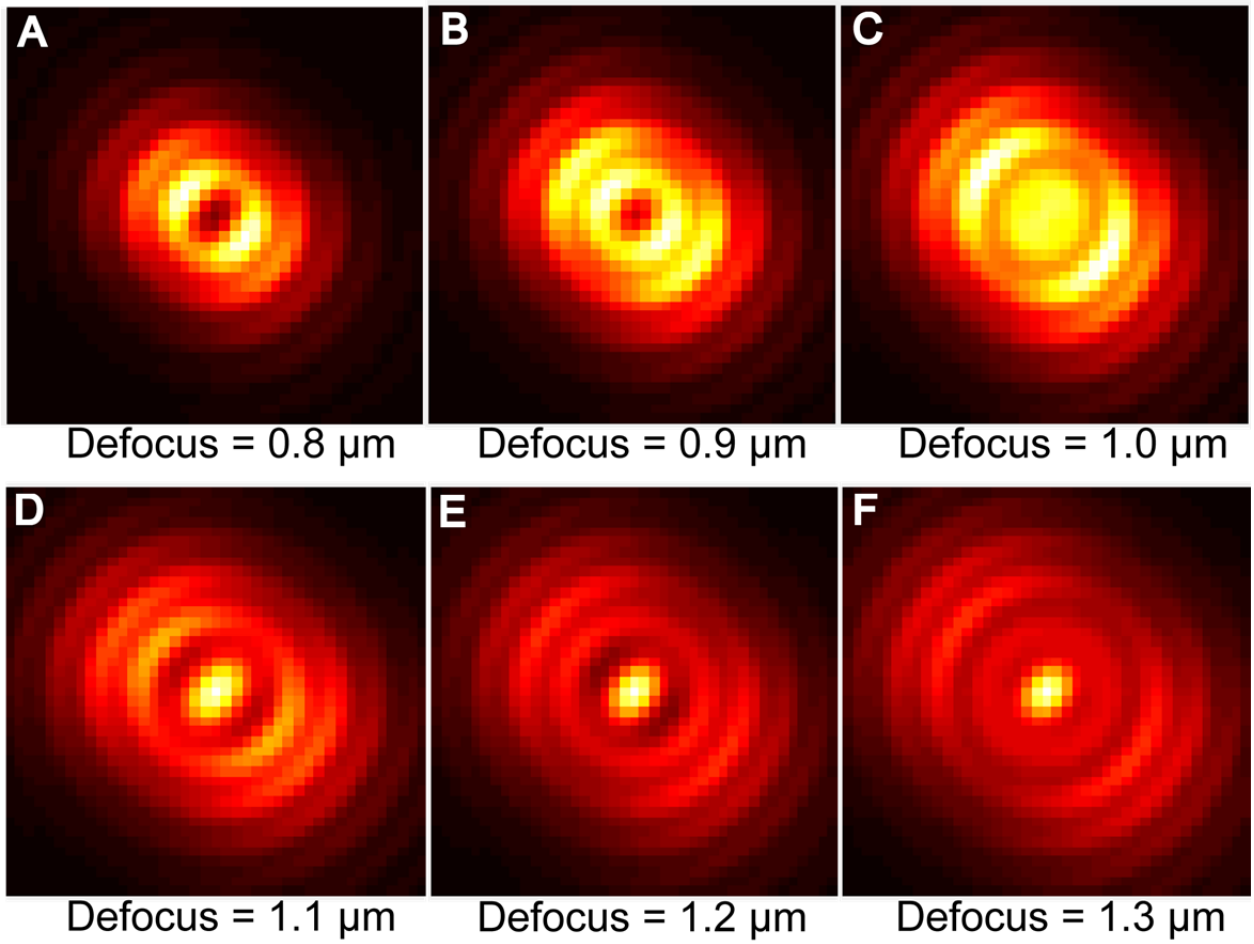

Supplemental Figure 1. Simulated defocused patterns of gold nanorods at θ = 0°. Patterns (A-F) are varied in their defocus depth by 100 nm to illustrate the effect of different defocus depths has on the recorded image.

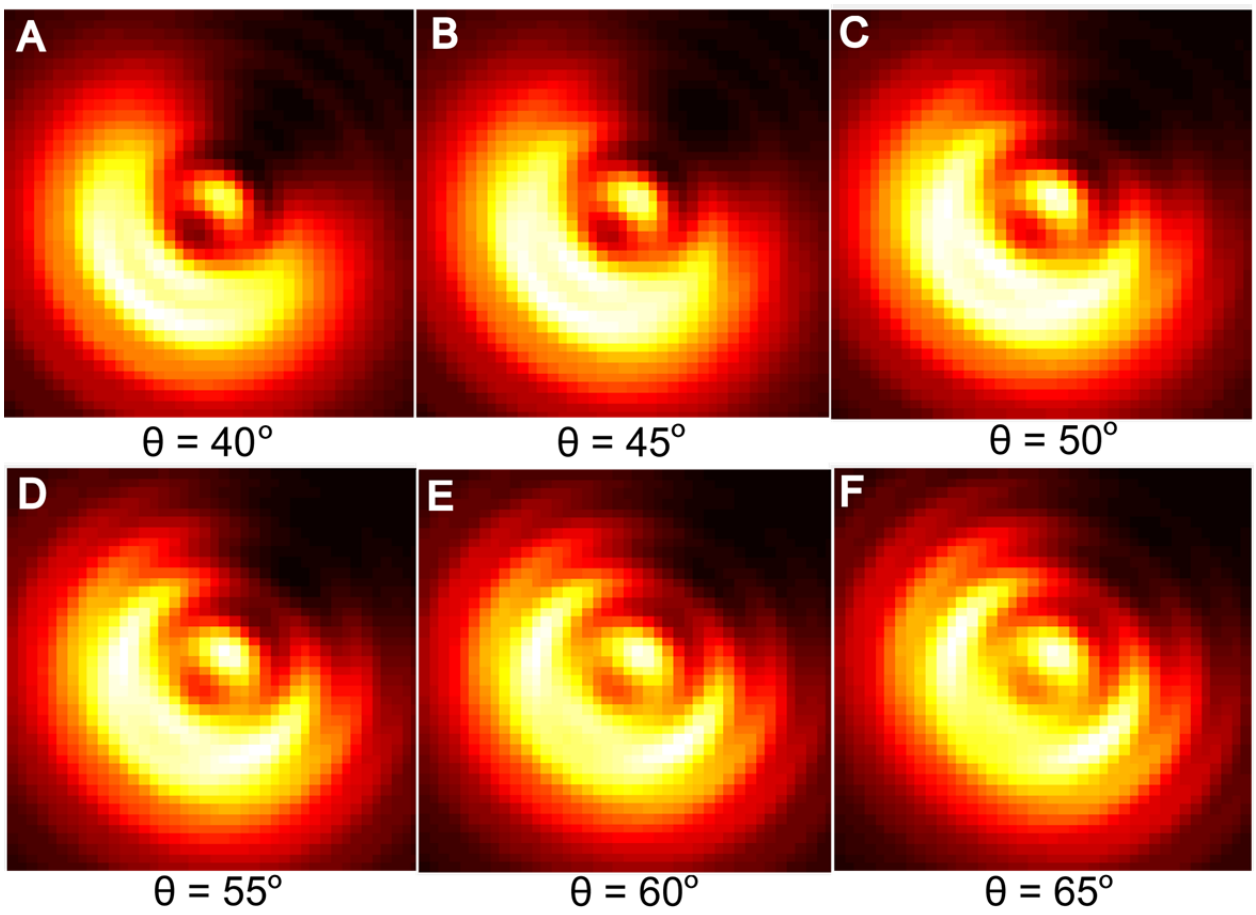

Supplemental Figure 2. Simulated defocused patterns of gold nanorods at polar angles varying from 40°-65°. All images were simulated with the same defocus depth of 1.0 μm. Presented to illustrate the difficulty in reliably assigning polar angles of tilted particles.

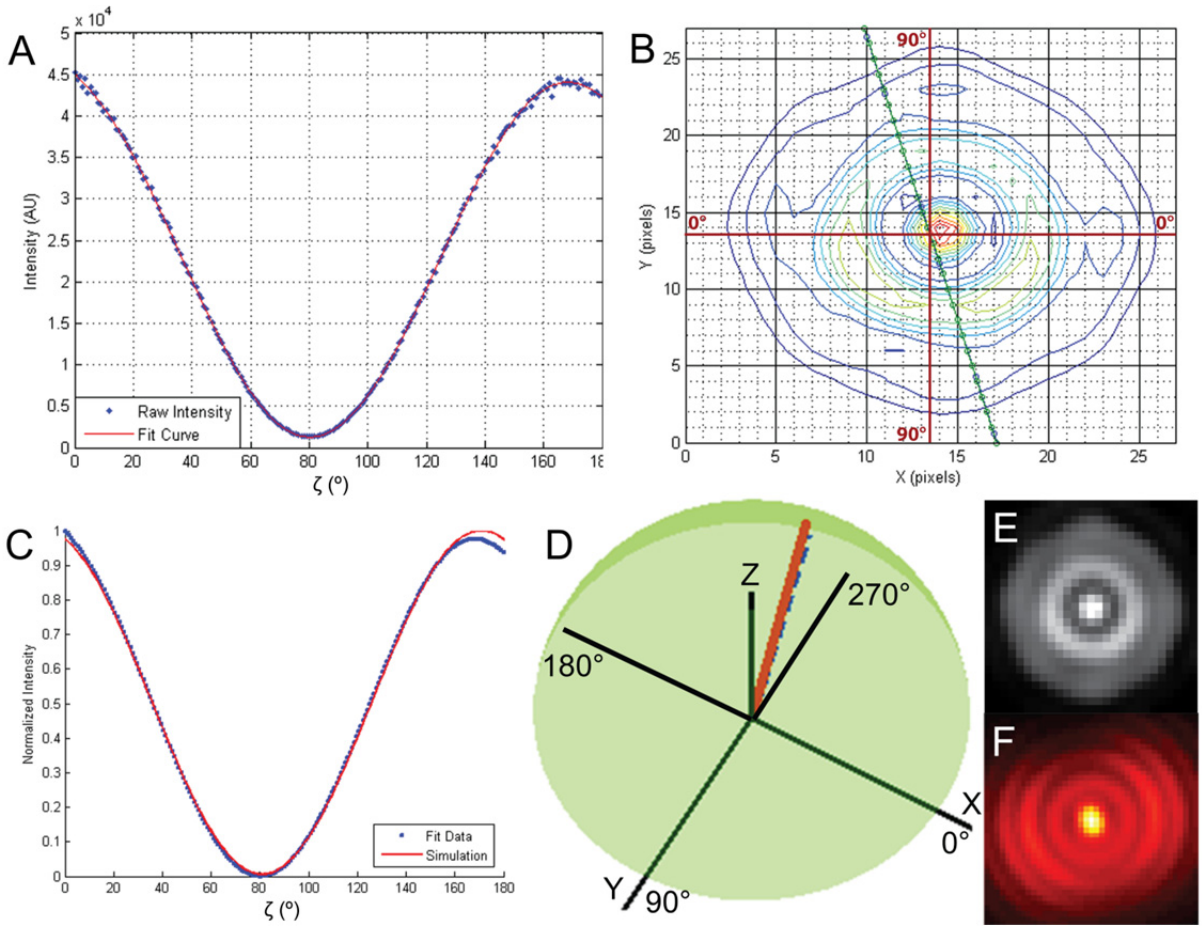

Supplemental Figure 3. Data and representations of a single AuNR with a polar angle of 81.5° ± 0.3°. (A) Raw intensity versus the first 180° of ζ fit with a higher-order polynomial. (B) Representation of the azimuthal angle determination using the defocused image with the highest contrast. The angle was determined to be 74.8° ± 2.7° with respect to the *x*-axis. (C) Plot portraying the alignment of the data with the simulated curves. (D) 3D representation of the AuNR in space. (E) Actual defocused imaged taken at the angle ζ of highest intensity. (F) Simulated image of a AuNR with the angles calculated for the particle (φ = 254.8°, θ = 81.5°).

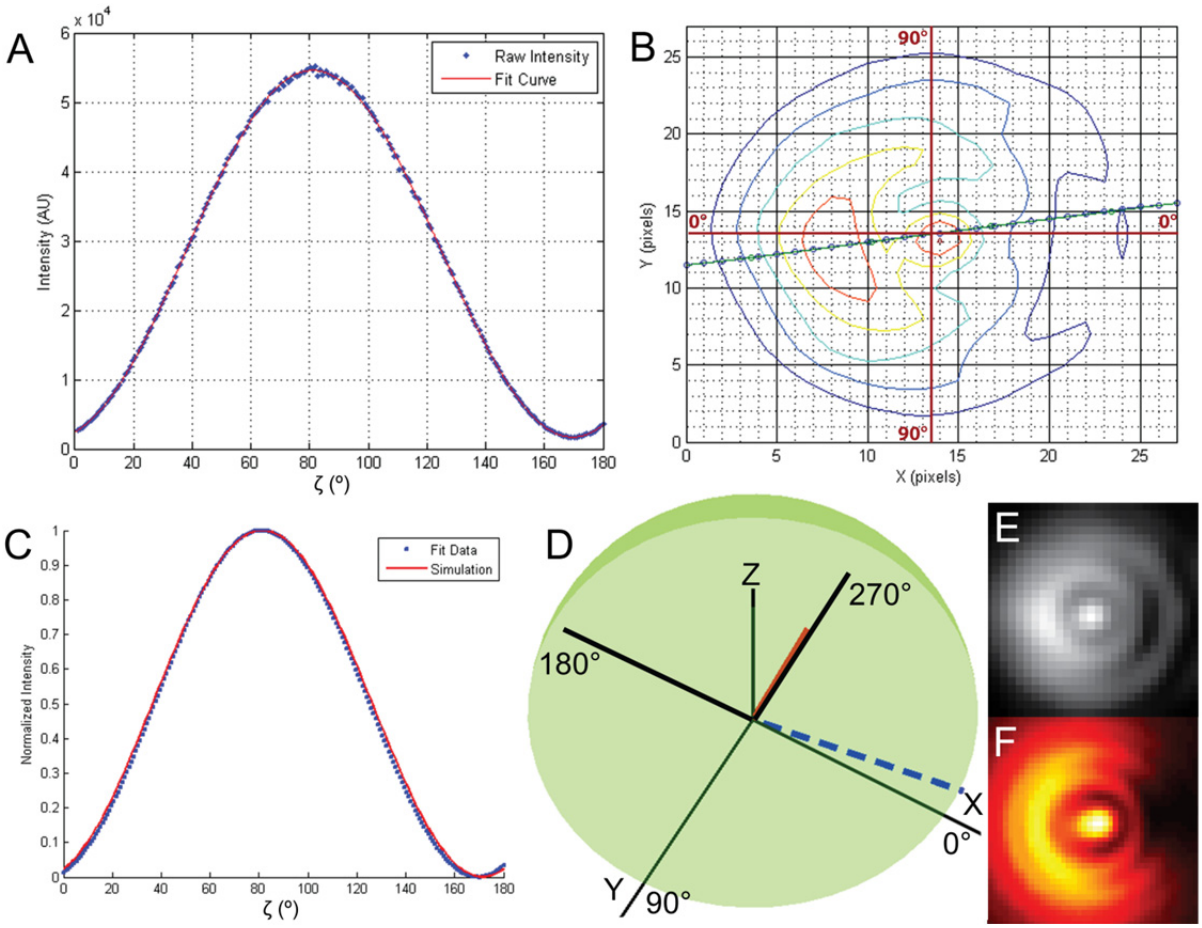

Supplemental Figure 4. Data and representations of a single AuNR with a polar angle of 48.3° ± 2.4°. (A) Raw intensity versus the first 180° ζ fit with a higher-order polynomial. (B) Representation of the azimuthal angle determination using the defocused image with the highest contrast. The angle was determined to be 8.6° ± 0.4° with respect to the *x*-axis. (C) Plot portraying the alignment of the data with the simulated curves. (D) 3D representation of the AuNR in space. (E) Actual defocused imaged taken at the angle ζ of highest intensity. (F) Simulated image of a AuNR with the angles calculated for the particle (φ = 351.4°, θ = 48.3°).

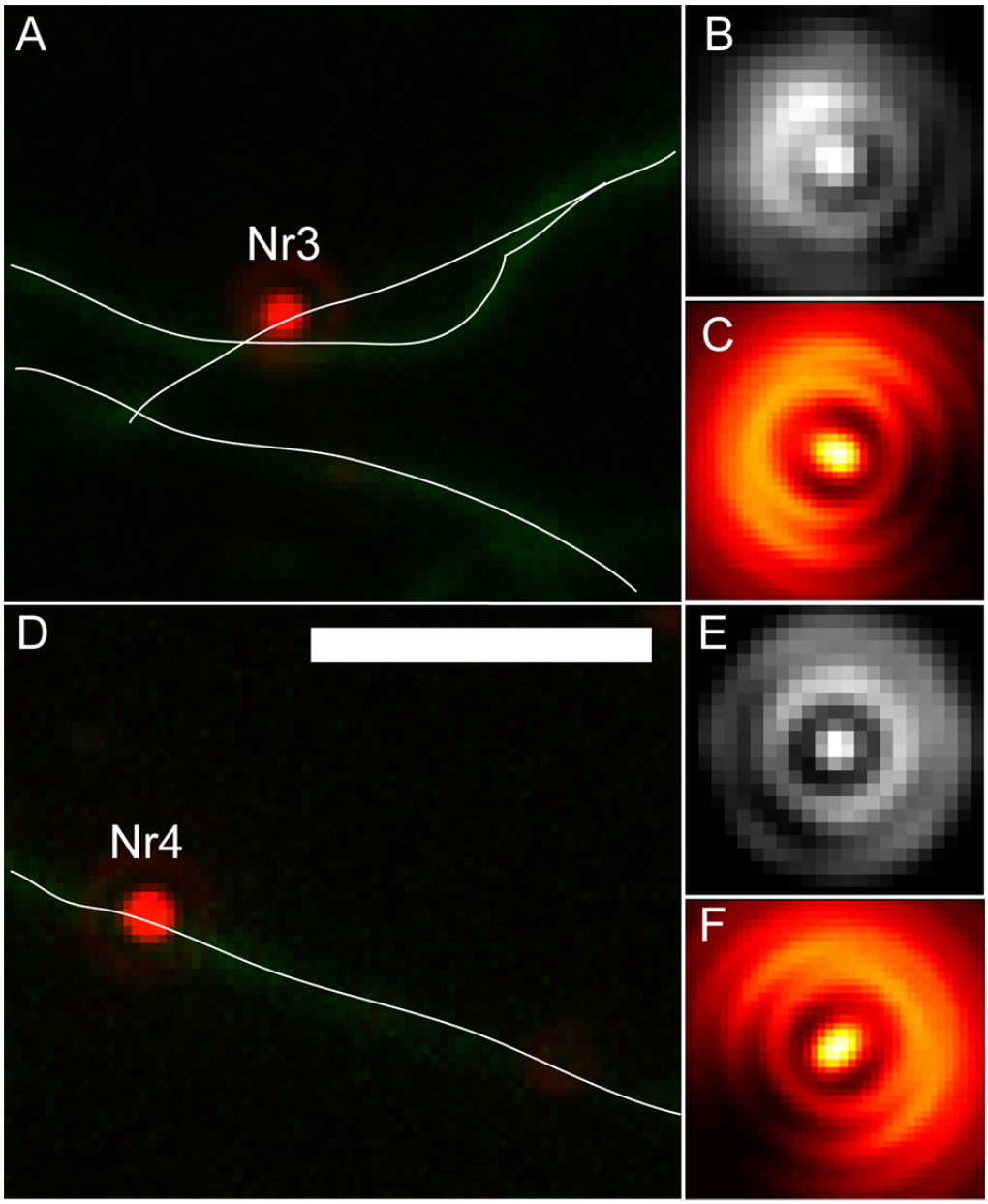

Supplemental Figure 5. Particles Nr3 and Nr4 attached to stationary microtubules and their corresponding defocused and simulated defocused images. Images in (B) and (C) correspond to Nr3 in (A), while (E) and (F) correspond to Nr4 in (D). Nr3 has a 3D orientation of $\varphi = 22.1° \pm 1.7°$ and $\theta = 59.3° \pm 2.7°$. Nr4 has a 3D orientation of $\varphi = 138.6° \pm 1.3°$ and $\theta = 55.9° \pm 1.5°$. Scale bar is 5 μm. White lines represent the approximate center of the microtubule fluorescence.

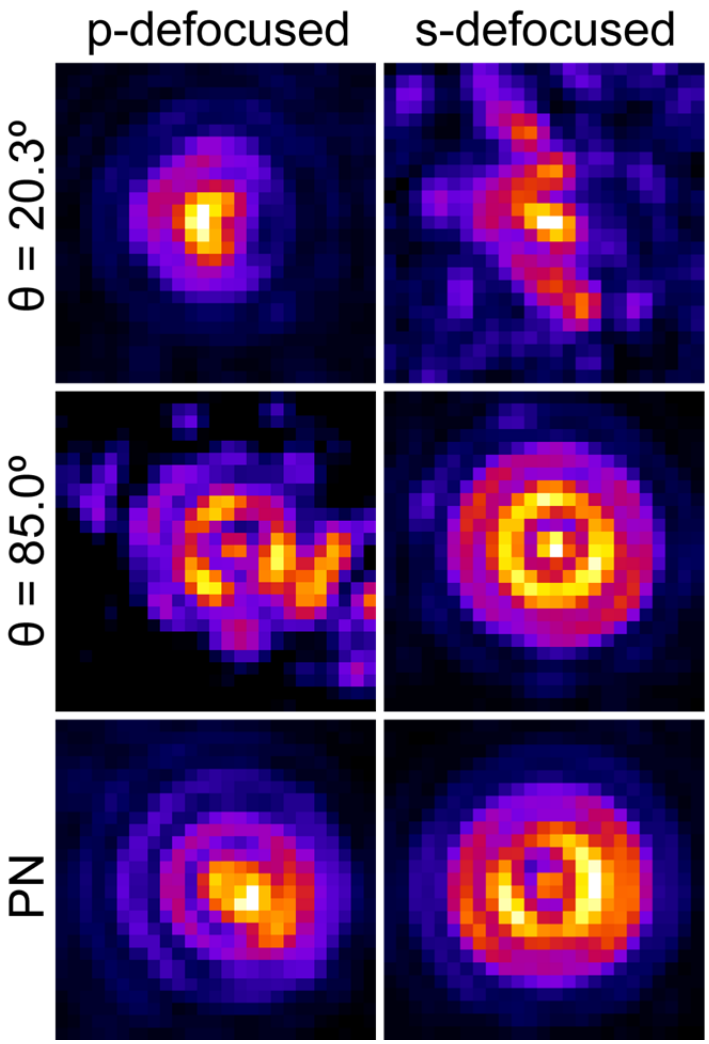

Supplemental Figure 6. Comparison of single particle and possible proximate neighbors (PN) with defocused imaging at p-pol and s-pol illumination. The top row shows a single particle with a polar angle of 20.3° and the second row shows a single particle with a polar angle of 85.0°. The bottom row displays what is considered a proximate neighbor at the two polarization illuminations.

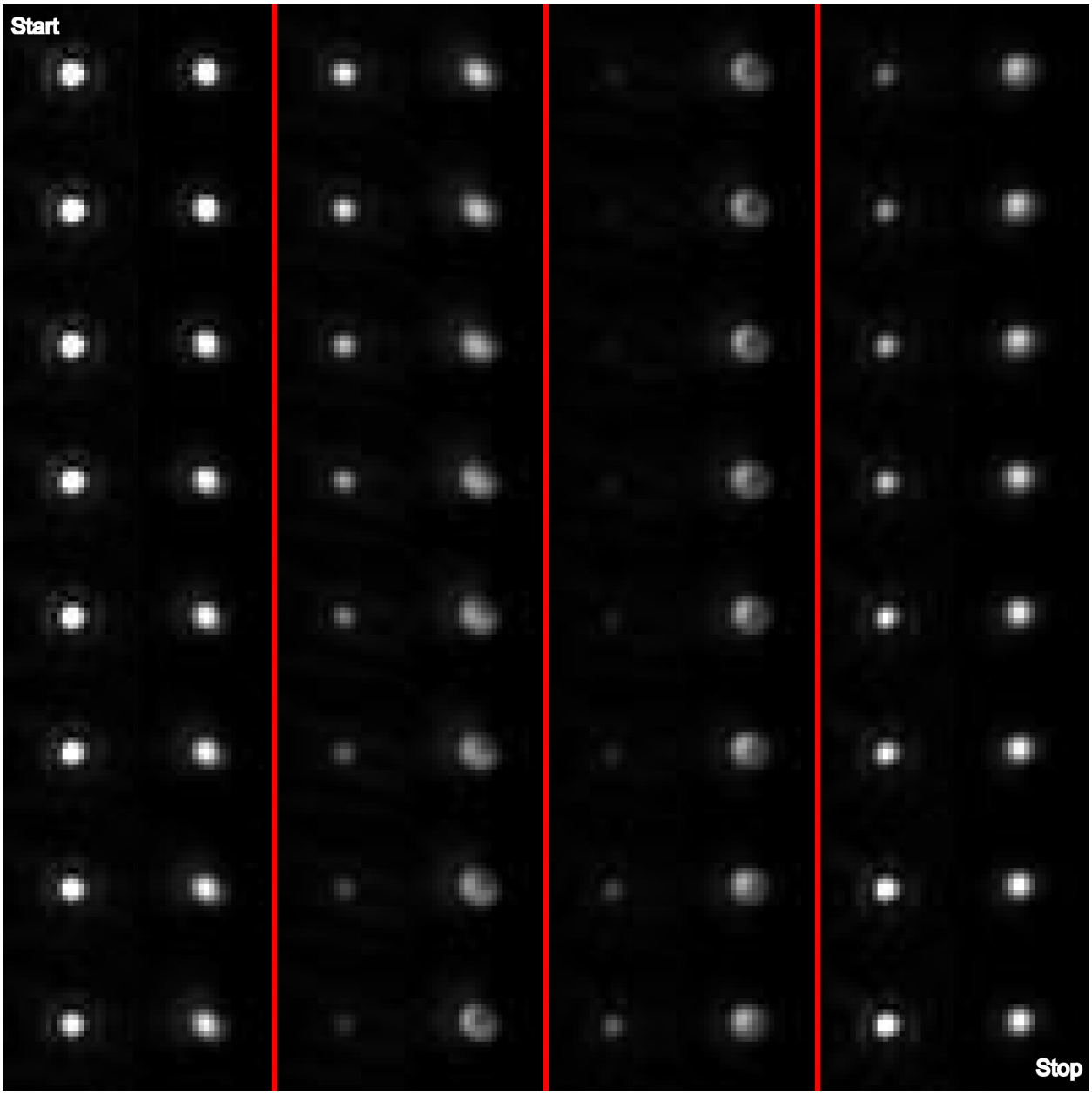

Supplemental Figure 7. Comparison of a single AuNR (left spot) with a large polar angle to a proximate neighbor (right spot) throughout a 180° rotation of ζ.